Mean-field phase diagram and spin-glass phase of the dipolar kagome Ising antiferromagnet

Leticia F. Cugliandolo

*Sorbonne Université, Laboratoire de Physique Théorique et Hautes Energies,
CNRS UMR 7589, 4, Place Jussieu, Tour 13, 5ème étage, 75252 Paris Cedex 05, France
and Institut Universitaire de France, 1 rue Descartes, 75231 Paris Cedex 05, France*

Laura Foini

Institut de Physique Théeorique, Université Paris Saclay, CNRS, CEA, F-91191 Gif-sur-Yvette, France

Marco Tarzia ⬤

*Sorbonne Université, Laboratoire de Physique Théeorique et Hautes Energies,
CNRS UMR 7589, 4, Place Jussieu, Tour 13, 5ème étage, 75252 Paris Cedex 05, France
and Institut Universitaire de France, 1 rue Descartes, 75231 Paris Cedex 05, France*

We derive the equilibrium phase diagram of the classical dipolar Ising antiferromagnet at the mean-field level on a geometry that mimics the two-dimensional kagome lattice. Our mean-field treatment is based on the combination of the cluster variational Bethe-Peierls formalism and the *cavity method*, developed in the context of the glass transition, and is complementary to the Monte Carlo simulations realized in a recent paper [Hamp *et al.*, Phys. Rev. B **98**, 144439 (2018)]. Our results confirm the nature of the low-temperature crystalline phase which is reached through a weakly first-order phase transition. Moreover, they allow us to interpret the dynamical slowing down observed in the work of Hamp *et al*. (referenced above) as a remnant of a spin-glass transition taking place at the mean-field level (and expected to be avoided in two dimensions).

I. INTRODUCTION

Many interesting classes of classical and quantum magnetic systems are extremely constrained. Hard local constraints lead to frustration and to the impossibility of satisfying all competing interactions simultaneously [1], giving rise to the existence of highly degenerate ground states [2,3]. Under certain conditions, these features produce a rich variety of collective behaviors [2,3], unconventional phase transitions [4,5], the emergence of a Coulomb phase with long-range correlations [6,7], and other remarkably unusual and exotic phenomena.

On the other hand, frustration is also one of the key properties of glassy systems [8–13], where it also arises from the fact that minimizing some local interactions leads to the impossibility of minimizing other ones [1]. This feature can generate rugged energy landscapes and slow dynamics even in the absence of disorder [14–31].

It is therefore surprising at first sight that very little is known on glassy phases in geometrically frustrated magnetic systems. One of the first tentative investigations on this subject has been performed in Ref. [32], where glassy behavior was observed in nonrandomly frustrated Ising models with competing interactions. More recently, strong nonequilibrium effects, slow dynamics, and super-Arrhenius relaxation have also been reported in two-dimensional spin systems with competing long- and short-range interactions [33,34].

On a different front, a thermodynamic theory, called the "frustration-limited domain theory" of the properties of supercooled liquids, and of the extraordinary increase of their characteristic structural relaxation times as the temperature is lowered, was formulated in terms of the postulated existence of a narrowly avoided thermodynamic phase transition due to geometric frustration [35] (see Ref. [19] for a review). In this context frustration describes an incompatibility between extension of the locally preferred order in a liquid and tiling of the whole space. This picture is consistent with appropriate minimal statistical mechanical models, such as three-dimensional (3D) Ising Coulomb frustrated lattice models, which display a slowing down of the relaxation in Monte Carlo simulations [18,36] and an ideal glass transition within mean-field approximations [18,20]. However, numerical simulations of these models in (3D) are limited by the presence of a first-order transition to a modulated, defect-ordered phase [18], and cannot be performed at sufficiently low temperatures.

Several frustrated spin (or Potts) lattice models without quenched disorder have also been introduced and studied over the past years to describe the key features of the glass transition. However, most of them are either mean field in nature (and cannot be easily generalized to finite dimensions) [14–16], or are characterized by (unphysical) multi-body interactions [31]. The classical three-coloring model on the two-dimensional (2D) hexagonal lattice has been shown to undergo a dynamical freezing in metastable states very similar to the one observed in structural glasses [37,38]. Slow dynamics also appears in electronic Coulomb liquids on the triangular lattice at quarter-filling [39], as well as in spin-ice systems both in 2D [40,41] and in 3D [42]. A sharp spin-glass transition has been observed in pyrochlore

oxides free of disorder [43,44], which is indistinguishable from the conventional one of the Edwards-Anderson model with quenched disorder [45]. On the quantum side, it was shown in Ref. [46] that a valence bond glass phase emerges in the SU(N) Hubbard-Heisenberg model on a Bethe lattice in the large-N limit due to the interplay of strong magnetic frustration and quantum fluctuations.

Yet, despite all these efforts over the past years, a clear and coherent picture of the glassy behaviors that can arise due to the effect of geometric frustration in finite-dimensional magnetic systems at low temperature is still missing.

Recently, Hamp *et al*. [47] studied an Ising model on the kagome lattice with short-range antiferromagnetic inter-actions and dipolar interactions decaying as $1/r^3$: the dipolar kagome Ising antiferromagnet (DKIAFM) introduced in [48]. By means of extensive Monte Carlo simulations, the authors first showed evidence for a first-order transition from the high-temperature paramagnetic phase to a low-temperature crystal state that breaks time-reversal and sublattice symmetries, and coincides with the one previously proposed in Ref. [48] as the ground state. Furthermore, upon cooling below the first-order transition, the system enters a supercooled liquid regime which exhibits all the characteristic features of fragile glasses: two-time autocorrelation functions decay as stretched exponentials and the relaxation time grows in a super-Arrhenius fashion as the temperature is decreased. However, these conclusions were drawn out of numerical simulations of relatively small systems (about 300 spins) and might be affected by both strong finite-size effects and the difficulty of reaching thermal equilibrium in a reliable fashion due to strong metastability effects. Moreover, a consistent picture of the physical origin of the dynamical slowing down at low temperatures has not been convincingly established yet.

In order to overcome, at least partially, these issues, in this paper we perform an analytical study of the equilibrium phase diagram of the DKIAFM in the thermodynamic limit at a mean-field level, focusing both on the ordered state and the glassy phase. Our results essentially confirm, support, and elucidate the observations reported in Ref. [47]. Upon decreasing temperature, we first find a transition to a sixfold-degenerate crystal state which breaks time-reversal and rotation sublattice symmetry as the one observed in [47,48]. The mean-field analysis indicates that the transition is indeed discontinuous. However, its first-order nature turns out to be "weak," in the sense that the spinodal point of the crystal phase is very close to the transition point, resulting in a very large jump of the specific heat at the transition. This feature provides a possible explanation of the fact that the finite-size scaling of the numerical data of the maximum of the specific heat with the system size performed in Ref. [47] did not find the usual behavior ($C_{\max} \propto N$) expected at a first-order transition due to very large finite-size effects.

When the system is supercooled below the first-order transition, we find that the paramagnetic state becomes unstable below a temperature at which the spin-glass susceptibility diverges. Here, a continuous spin-glass transition takes place at the mean-field level [49].

Note that the fact that the model displays a continuous spin-glass transition in mean-field instead of a random first-order transition [50,51] of the kind found in structural glasses

(such as hard spheres in infinite dimensions [27] and lattice glass models on the Bethe lattice [21,22,24–26]) is perhaps not surprising. In fact, Ising spins with antiferromagnetic couplings on high-dimensional frustrated lattices and other related frustrated mean-field models with pairwise interactions are known to undergo a continuous transition to a spin-glass phase when the temperature is lowered below the critical temperature of the antiferromagnetic phase [26,52]. In this respect, it is interesting to notice that a spin-glass transition has been recently found theoretically in a model of disorder-free pyrochlore magnets [44] introduced to clarify the origin of the spin-glass transition observed in the experiments on pyrochlore magnets [43]. The model consists of spin and orbital degrees of freedoms which induce effective dynamical randomness on each other, and simultaneously freeze into the disordered state.

Beyond the fact that both spin glasses and structural glasses exhibit a pronounced slowing down of the dynamics upon cooling and aging in the low-temperature phase, several important qualitative and quantitative differences characterize the dynamical behavior of these systems: In structural glasses, two-time autocorrelation functions generically exhibit a two-step relaxation, characterized by a relatively fast decay to a plateau (i.e., the Edwards-Anderson order parameter) which appears discontinuously upon lowering the temperature, followed by a much slower decay, described by a stretched exponential. Moreover, the structural relaxation time is found to grow extremely fast, in a super-Arrhenius fashion, as the temperature is decreased [8–13]. Conversely, in spin glasses the Edwards-Anderson order parameter is continuous at the transition and vanishes in the paramagnetic phase. Hence, two-time autocorrelation functions should display a simple exponential decay when the transition is approached from the high-temperature phase, and an algebraic decay at the critical point. Furthermore, the relaxation time is expected to diverge (only) as a power law at the critical point (and to stay infinite in the whole low-temperature phase) [49]. Nonetheless, these differences are not clearly visible in numerical simulation of relatively small samples. A clear example of that is provided by the analysis of the dynamics of 3D Ising spin glasses performed in Refs. [53,54] using Monte Carlo simulations of systems with up to 64^3 spins. The two-time autocorrelation function was found to be very well fitted by stretched exponentials, with an exponent β that exhibits a temperature dependence extremely similar to the one reported in [47] for the DKIAFM. Moreover, although the divergence of the relaxation time as a power law $\tau \sim (T - T_c)^{-z\nu}$ is consistent with the numerics, a Vogel-Fulcher law $\tau \sim e^{E_0/(T-T_c)}$ was also found to account reasonably well for the data. These observations clearly illustrate that, although the origin of stretched exponential relaxations in the 3D Edwards-Anderson model and in fragile glass formers is of different nature, making a clear distinction between a spin glass and a glass type of dynamical slowing down is not always an easy task when analyzing numerical data of finite-size samples.

The lower-critical dimension of the spin-glass transition is expected to be $d_L \approx 2.5$ [55] (at least in the case of short-range interactions). Hence, on general grounds we do not expect a genuine spin-glass phase for the DKIAFM in 2D.

Yet, the manifestations of the vestige of the transition can be very strong also in two-dimensional systems: The spin-glass amorphous order can establish over very long (although not infinite) length scales, the spin-glass susceptibility can become very large (although not infinite), and the relaxation time can grow very fast at low temperature. Several experimental realizations of two-dimensional spin glasses using thin films do indeed show the same behavior as 3D spin glasses at sufficiently low temperature [56–58]. In this sense, the existence of the spin-glass phase in higher dimension, accompanied by the growth of long-range amorphous order and a rough free-energy landscape, provides a possible and natural explanation of the slow dynamics observed in the numerical simulations of Ref. [47] of the 2D model at low temperatures.

Despite the fact that our mean-field approach consists in studying the model on a random sparse graph of triangular kagome plaquettes, and cutting off the dipolar interactions beyond the second-nearest-neighbor plaquettes (i.e., the fifth-nearest-neighbor spins), it provides a remarkably good approximation for the equilibrium properties of the 2D DKIAFM. For instance, the mean-field approach yields a zero-temperature entropy density of the nearest-neighbor kagome spin-ice model obtained for $D = 0$ [59] equal to $s_{GS} \approx 0.752\,04$, which turns out to be extremely close to the Pauling estimate $s_{GS} \approx 0.752\,25$. Similarly, the ground-state energy density of the crystal ground state within the mean-field approximation is $e_{GS} \approx -1.6116$, which accounts reasonably well for the one found in the Monte Carlo simulations of systems with 300 spins, $e_{GS} \approx -1.515$ [60]. As expected, the transition temperature to the crystalline phase is overestimated (by about a factor 3) by the mean-field treatment. Yet, the temperature dependence of the specific heat, the energy density, and the magnetization are remarkably similar, also at a quantitative level, to the ones found with Monte Carlo simulations (see Fig. 3).

The results presented here can serve at least two purposes: (i) They help to support, understand, and clarify the numerical results of Ref. [47]. (ii) They provide a first step to bridge the gap between the slow dynamics observed in geometrically frustrated magnetic systems and the theory of the glass transition formulated in terms of rough free-energy landscapes. We believe that this analysis is of particular interest, especially in the light of the experimental relevance of the model, which could be potentially realized in several realistic setups, including colloidal crystals [61,62], artificial nanomagnetic arrays [63,64], cold polar molecules [65], atomic gases with large magnetic dipole moments [66], and layered bulk kagome materials [67–69].

The paper is organized as follows. In the next section we introduce the model. In Sec. III we describe the mean-field approach, based on a cluster formulation of the problem on the Bethe lattice. In Sec. IV we show the results found within our analytical treatment, including the phase diagram and the equation of state. Finally, in Sec. V we provide some concluding remarks and perspectives for future work. In the Appendix A we discuss the solution of the antiferromagnetic Ising model on the Bethe lattice which can be useful to understand the results obtained for the DKIAFM in a simpler setting.

II. MODEL

We consider the DKIAFM [47,48] in which N classical spins $S_i = \pm 1$ are placed on the vertices of a two-dimensional kagome lattice and point in a direction perpendicular to the plane. The Hamiltonian comprises an antiferromagnetic exchange term of strength J between spins at nearest-neighbor lattice sites $\langle ij \rangle$ and long-range dipolar interactions of characteristic strength D between all pairs of spins:

$$\mathcal{H} = J \sum_{\langle ij \rangle} S_i S_j + \frac{D}{2} \sum_{i \neq j} \frac{S_i S_j}{r_{ij}^3}, \tag{1}$$

where the distance $r_{ij} = |\mathbf{r}_i - \mathbf{r}_j|/a$ between the spins i and j is measured in units of the lattice spacing a (that we set equal to 1 throughout).

In the following, we will be interested in the case in which both interactions are antiferromagnetic, i.e., $J > 0$ and $D > 0$. The case $D = 0$ is known to be fully frustrated and does not order down to zero temperature [70]. The phase diagram of the $J = 0$ model is less well understood but the system is again strongly frustrated with any ordering (if present at all) suppressed down to temperatures $T \ll D$ [63].

The previous studies of the model [47,48] considered the coupling parameters $D = 1$ K and $J = 0.5$ K (setting $k_B = 1$ and measuring all energies in Kelvin). A further advantage of developing an analytic (although approximate) treatment is that it is relatively simple to explore the parameter space. Without loss of generality, we set $J = 0.5$ K throughout (as in [47,48]) and study the phase diagram of the model and the constitutive equations in the different phases varying the dipolar coupling D and the temperature T.

III. MEAN-FIELD ANALYSIS

Our mean-field treatment is based on the combination of the cluster variational Bethe-Peierls formalism (already successfully employed in the study of the equilibrium properties of geometrically frustrated magnetic systems [4,71–74]) and the *cavity method* [52], developed in the context of glassy and disordered systems described by replica symmetry breaking (RSB). The latter concept is related to a complex free-energy landscape with special structure and the calculational meaning of it, in the context of the cavity method, will become clear below.

This long (and rather technical) section is organized as follows: In the next subsection we motivate the choice of the treelike lattice of triangular plaquettes used in the calculation, the random regular graph (RRG). In Sec. III B we show how to obtain the recursion relations for the local probabilities of finding specific spin configurations on each plaquette. In Sec. III C we explain the solution of these equations in the simplest high-temperature paramagnetic phase, and discuss the stability of this solution in Sec. III D. In Sec. III E we describe the crystalline phase, found on a modified eight-partite RRG built in such a way that the specific spatial structure of the ground state proposed in Refs. [47,48] can establish. Finally, in Sec. III F we discuss the existence of a spin-glass phase at low temperature described by RSB. The reader who is not interested in the technical details can skip

this whole section and jump to Sec. IV, with the discussion of the phase diagram.

A. Random regular graph

Originally, the Bethe approximation was introduced on (loopless) Cayley trees of fixed connectivity. These graphs have no loops by definition and have (roughly) half of the sites lying on the boundary (i.e., the leaves of the tree). The hierarchical structure of the lattice allows one to obtain exact recursion relations which can be solved by iterations starting from some initial condition on the leaves. When studying homogeneous phases or, more generally, situations where the Gibbs measure is characterized by a single, or few, pure states, the recursion equations converge after a few iterations (the number of which may depend on the proximity to a critical point) to a stationary solution in the bulk of the tree, which is independent of the initial condition. Then, thermodynamic observables are measured in this bulk region, close to the root.

However, this approach fails if the Gibbs measure breaks into a large number of pure states (i.e., local minima of the free energy), which is precisely what happens in glasses and spin glasses in mean field. This has been transparently understood by Mézard and Parisi [52], who managed to solve the problem and to obtain the correct physical description of glassy phases on sparse random networks. The issue when the number of local minima of the free energy proliferates is that, since on a Cayley tree a finite fraction of the sites sits on the boundary, the choice of the initial conditions for the recursion equations fix the solution that one finds in the bulk (which never converges to a stationary value). The correct way to average over all possible pure states is to get rid of the boundaries and treat them self-consistently. This is done by introducing random regular graphs (RRGs), which are essentially trees wrapped onto themselves. RRGs are a special class of sparse graphs (i.e., a set of nodes and edges connecting them), whose elements are chosen at random with uniform probability over the ensemble of all graphs such that each node has exactly $k + 1$ neighbors. The properties of these graphs have been extensively studied in the latest years (for a review see [75]). The most relevant property in this context is the fact that RRGs do (necessarily) have loops, but their typical length scales as the logarithm of the total number of nodes. This implies that in the thermodynamic limit, the size of the loops diverges and the RRG looks locally like a tree, which makes the recursion relations asymptotically exact.

Hence, an RRG is locally a tree, but it is frustrated, does not have a boundary, is statistically translational invariant, and, as we will explain later, allows one to self-consistently average over all possible free-energy minima by taking into account their Gibbs weight. For these reasons, RRGs are the suitable geometric structures to study the thermodynamics of glassy and disordered systems at a mean-field level [21,22,24,25] (i.e., in the limit of infinite dimensions).

In order to combine the cavity method and the cluster variational approach for the DKIAFM, hereafter we study the model (1) on an (infinite) RRG of N_Δ triangular plaquettes of total coordination three (see Fig. 1 for a sketch). In this case, the number of spins is equal to $N = 3N_\Delta/2$ since each spin belongs to two plaquettes and each plaquette contains three spins.
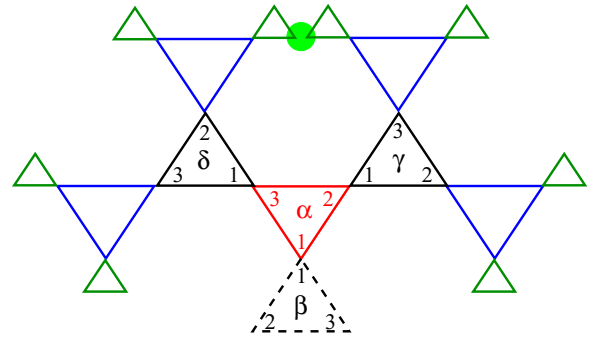

FIG. 1. Sketch of a small portion of a (rooted) random regular graph (RRG) of triangular plaquettes in presence of a cavity (the dashed black plaquette β). Each up-type triangular plaquette of the RRG is connected to three down-type triangular plaquettes and each down-type triangular plaquette is connected to up down-type triangular plaquettes. The graph looks locally like a tree since typical loops are very large (the typical size of the loops diverges as $\log N_\Delta$). The first-nearest-neighboring plaquettes (β, γ, and δ) of the central (red) triangle (α) are drawn in black, the second-nearest-neigboring plaquettes in blue, and the third-nearest-neighboring plaquettes in green. The mean-field Bethe-Peierls approximation consists in discarding the fact that the two spins inside the green circle are in fact the same spin on the original kagome lattice. Moreover the dipolar coupling is cut off beyond the second-nearest-neighboring plaquettes (i.e., fifth-nearest-neighbor spins).

B. "Cavity" recursion relations

The standard way to obtain the recursion relations for the marginal probabilities of observing a given spin configuration on a given plaquette is provided by the *cavity method* [52], which is equivalent to the Bethe-Peierls approximation at the replica-symmetric level. The cavity method is based on the assumption that, due to the treelike structure of the lattice, in absence of a given plaquette (the *cavity*, e.g., the red triangle of Fig. 1), the neighboring plaquettes (the black triangles of Fig. 1) are uncorrelated and their marginal joint probabilities factorize. (Throughout the paper we will use the words "triangle" and "plaquette" indistinctly.) Thanks to such factorization property one can write relatively simple recursion equations for the marginal probabilities of the cavity sites. Such equations have to be solved self-consistently, the fixed points of which yield the free energy of the system along with all the thermodynamic observables (all the technical details of the method can be found in Refs. [24,52]). However, in order to be tractable, the cavity approach is formulated for systems with finite-range interactions. Hence, before proceeding further we need to treat the dipolar interactions of Eq. (1) in an approximate fashion. In practice, in the analytic calculations described below we choose to cut off the dipolar couplings up to second-nearest-neighboring plaquettes (i.e., the interactions between the spins belonging to the red plaquette α of Fig. 1 and the spins belonging to green plaquettes are set to zero).

Consider now the triangle α (red) in absence of the interactions with the spins belonging to one of its neighboring plaquettes β (dashed black). We define $p_{\alpha \to \beta}(\{S_\alpha\}|\{S_\beta\})$ as the probability to observe the spin configuration $\{S_\alpha\} \equiv \{S_{\alpha,1}, S_{\alpha,2}, S_{\alpha,3}\}$ on the triangle α of the (rooted) RRG with the cavity β, given that the spin configuration of the plaquette

β is $\{S_\beta\} \equiv \{S_{\beta,1}, S_{\beta,2}, S_{\beta,3}\}$. We have adopted the convention that spin 1 is the root of the cavity plaquette and spins 2 and 3 are labeled anticlockwise. Using this convention, one has that $S_{\beta,1} \equiv S_{\alpha,1}$.

The probabilities $p_{\alpha\to\beta}(\{S_\alpha\}|\{S_\beta\})$ can be written in terms of the marginal probabilities defined on the triangles γ and δ in absence of the (cavity) triangle α, times the Gibbs' weight associated to each spin configuration:

$$p_{\alpha\to\beta}(\{S_\alpha\}|\{S_\beta\}) = \left(\mathcal{Z}_{\alpha\to\beta}^{(\text{iter})}\right)^{-1} \sum_{\llcorner\gamma,\delta\lrcorner_\alpha} p_{\gamma\to\alpha}(\{S_\gamma\}|\{S_\alpha\}) \, p_{\delta\to\alpha}(\{S_\delta\}|\{S_\alpha\}) \, e^{-\beta\tilde{\mathcal{H}}_{\alpha\to\beta}(\{S_\alpha,S_\gamma,S_\delta\}|\{S_\beta\})}, \tag{2}$$

where $\mathcal{Z}_{\alpha\to\beta}^{(\text{iter})}$ is a normalization factor ensuring that $\sum_{\{S_\alpha\},\{S_\beta\}} p_{\alpha\to\beta}(\{S_\alpha\}|\{S_\beta\}) = 1$ and is associated to the "free-energy shift" involved in the iteration process: $-\beta\Delta F_{\alpha\to\beta}^{(\text{iter})} \equiv \log \mathcal{Z}_{\alpha\to\beta}^{(\text{iter})}$. Here, we introduce the notation $\sum_{\llcorner\gamma,\delta\lrcorner_\alpha}$ that indicates the sum over all possible configurations $\{S_\gamma\}$ and $\{S_\delta\}$ of the spin degrees of freedom of the plaquettes γ and δ, compatible with the constraints imposed by the spin configuration $\{S_\alpha\}$ on the plaquette α, i.e., $S_{\gamma,1} = S_{\alpha,2}$ and $S_{\delta,1} = S_{\alpha,3}$ [see Eq. (10)]. We will use this notation throughout this section. The Hamiltonian $\tilde{\mathcal{H}}_{\alpha\to\beta}(\{S_\alpha, S_\gamma, S_\delta\}|\{S_\beta\})$ appearing in the Gibbs factor of Eq. (2) is a modified Hamiltonian, Eq. (1), restricted to the plaquette $\alpha \to \beta$ with the missing neighboring plaquette β:

$$\tilde{\mathcal{H}}_{\alpha\to\beta}(\{S_\alpha, S_\gamma, S_\delta\}|\{S_\beta\}) \equiv \mathcal{H}_\alpha^{(\text{AF})} + \tilde{\mathcal{H}}_{\gamma\to\alpha}^{(\text{2D})} + \tilde{\mathcal{H}}_{\delta\to\alpha}^{(\text{3D})} + \tilde{\mathcal{H}}_{(\gamma,\delta)}^{(\text{2NND})} + \tilde{\mathcal{H}}_{(\gamma,\beta)}^{(\text{2NND})} + \tilde{\mathcal{H}}_{(\delta,\beta)}^{(\text{2NND})},$$

$$\mathcal{H}_\alpha^{(\text{AF})} = (J + D)[S_{\alpha,1}S_{\alpha,2} + S_{\alpha,1}S_{\alpha,3} + S_{\alpha,2}S_{\alpha,3}],$$

$$\tilde{\mathcal{H}}_{\gamma\to\alpha}^{(\text{2D})} = D\left[\frac{S_{\alpha,1}S_{\gamma,2} + S_{\alpha,3}S_{\gamma,3}}{3\sqrt{3}} + \frac{S_{\alpha,1}S_{\gamma,3} + S_{\alpha,3}S_{\gamma,2}}{8}\right],$$

$$\tilde{\mathcal{H}}_{\delta\to\alpha}^{(\text{3D})} = D\left[\frac{S_{\alpha,1}S_{\delta,3} + S_{\alpha,2}S_{\delta,2}}{3\sqrt{3}} + \frac{S_{\alpha,1}S_{\delta,2} + S_{\alpha,2}S_{\delta,3}}{8}\right],$$

$$\tilde{\mathcal{H}}_{(\gamma,\delta)}^{(\text{2NND})} = D\left[\frac{S_{\gamma,3}S_{\delta,2}}{8} + \frac{S_{\gamma,2}S_{\delta,2} + S_{\gamma,3}S_{\delta,3}}{7\sqrt{7}} + \frac{S_{\gamma,2}S_{\delta,3}}{27}\right]. \tag{3}$$

The meaning of this decomposition is the following. $\tilde{\mathcal{H}}_{\gamma\to\alpha}^{(\text{2D})}$ contains the four dipolar interaction terms between the spins belonging to the plaquette α and the spin belonging to its nearest-neighbor plaquette γ attached to the spin $S_{\alpha,2}$, which are not already contained in $\mathcal{H}_\alpha^{(\text{AF})}$. $\tilde{\mathcal{H}}_{(\gamma,\delta)}^{(\text{2NND})}$ contains the four dipolar interaction terms between the spins of the second-nearest-neighbor plaquettes γ and δ which are not already contained in $\tilde{\mathcal{H}}_{\gamma\to\alpha}^{(\text{2D})}$ and $\tilde{\mathcal{H}}_{\delta\to\alpha}^{(\text{3D})}$.

In order to obtain the marginal probabilities of the spin configurations on each plaquette of the (unrooted) RRG (where each triangular plaquette has exactly three neighbors), one needs to merge three plaquettes with a cavity (e.g., plaquettes β, γ, and δ of Fig. 1) onto their neighboring plaquette (e.g., plaquette α of Fig. 1). In this way, one obtains

$$P_\alpha(\{S_\alpha\}) = \left(\mathcal{Z}_\alpha^{(s)}\right)^{-1} \sum_{\llcorner\beta,\gamma,\delta\lrcorner_\alpha} p_{\beta\to\alpha}(\{S_\beta\}|\{S_\alpha\}) \, p_{\gamma\to\alpha}(\{S_\gamma\}|\{S_\alpha\}) \, p_{\delta\to\alpha}(\{S_\delta\}|\{S_\alpha\}) \, e^{-\beta\tilde{\mathcal{H}}_\alpha(\{S_\alpha,S_\beta,S_\gamma,S_\delta\})}, \tag{4}$$

where $\mathcal{Z}_\alpha^{(s)}$ is a normalization factor ensuring that $\sum_{\{S_\alpha\}} P_\alpha(\{S_\alpha\}) = 1$, and is associated to the "free-energy shift" involved in the process of joining three plaquettes (β, γ, and δ) to a central cavity plaquette (α): $-\beta\Delta F_\alpha^{(s)} \equiv \log \mathcal{Z}_\alpha^{(s)}$. The plaquette Hamiltonian $\tilde{\mathcal{H}}_\alpha(\{S_\alpha, S_\beta, S_\gamma, S_\delta\})$ reads as

$$\tilde{\mathcal{H}}_\alpha(\{S_\alpha, S_\beta, S_\gamma, S_\delta\}) \equiv \mathcal{H}_\alpha^{(\text{AF})} + \tilde{\mathcal{H}}_{\beta\to\alpha}^{(\text{1D})} + \tilde{\mathcal{H}}_{\gamma\to\alpha}^{(\text{2D})} + \tilde{\mathcal{H}}_{\delta\to\alpha}^{(\text{3D})} + \tilde{\mathcal{H}}_{(\gamma,\delta)}^{(\text{2NND})} + \tilde{\mathcal{H}}_{(\gamma,\beta)}^{(\text{2NND})} + \tilde{\mathcal{H}}_{(\delta,\beta)}^{(\text{2NND})},$$

$$\tilde{\mathcal{H}}_{\beta\to\alpha}^{(\text{1D})} = D\left[\frac{S_{\alpha,2}S_{\beta,3} + S_{\alpha,3}S_{\beta,2}}{3\sqrt{3}} + \frac{S_{\alpha,2}S_{\beta,2} + S_{\alpha,3}S_{\beta,3}}{8}\right], \tag{5}$$

and the other terms are given in Eq. (3).

The equilibrium averages of all local observables which involve the spin degrees of freedom of a given plaquette, including, e.g., the magnetization, can be expressed in terms of these marginal probabilities:

$$\langle O_\alpha\rangle = \sum_{\{S_\alpha\}} O(\{S_\alpha\}) P_\alpha(\{S_\alpha\}). \tag{6}$$

Similarly, the contribution to the average energy due to the plaquette α can be expressed as

$$\langle e_\alpha^{(s)}\rangle = \frac{\sum_{\llcorner\alpha\to(\beta,\gamma,\delta)\lrcorner} p_{\beta\to\alpha}(\{S_\beta\}|\{S_\alpha\}) \, p_{\gamma\to\alpha}(\{S_\gamma\}|\{S_\alpha\}) \, p_{\delta\to\alpha}(\{S_\delta\}|\{S_\alpha\}) \, \tilde{\mathcal{H}}_\alpha(\{S_\alpha, S_\beta, S_\gamma, S_\delta\}) \, e^{-\beta\tilde{\mathcal{H}}_\alpha(\{S_\alpha,S_\beta,S_\gamma,S_\delta\})}}{\sum_{\llcorner\alpha\to(\beta,\gamma,\delta)\lrcorner} p_{\beta\to\alpha}(\{S_\beta\}|\{S_\alpha\}) \, p_{\gamma\to\alpha}(\{S_\gamma\}|\{S_\alpha\}) \, p_{\delta\to\alpha}(\{S_\delta\}|\{S_\alpha\}) \, e^{-\beta\tilde{\mathcal{H}}_\alpha(\{S_\alpha,S_\beta,S_\gamma,S_\delta\})}}. \tag{7}$$

The process of joining two neighboring plaquettes (each one being a cavity for the other) (e.g., plaquettes α and β of Fig. 1) involves another "free-energy shift," defined as

$$e^{-\beta \Delta F_{\alpha \leftrightarrow \beta}^{(l)}} \equiv \mathcal{Z}_{\alpha \leftrightarrow \beta}^{(l)} = \sum_{\llbracket \alpha \leftrightarrow \beta \rrbracket} p_{\alpha \to \beta}(\{S_\alpha\}|\{S_\beta\})\, p_{\beta \to \alpha}(\{S_\beta\}|\{S_\alpha\})\, e^{-\beta \tilde{\mathcal{H}}_{\beta \to \alpha}^{(\mathrm{1D})}}, \tag{8}$$

where the Gibbs' factor $\tilde{\mathcal{H}}_{\beta \to \alpha}^{(\mathrm{D})}$ has been defined in Eq. (5). Similarly, the contribution to the average energy coming from the interactions between two neighboring plaquettes is given by

$$\langle e_{\alpha \leftrightarrow \beta}^{(l)} \rangle = \frac{\sum_{\llbracket \alpha \leftrightarrow \beta \rrbracket} p_{\alpha \to \beta}(\{S_\alpha\}|\{S_\beta\})\, p_{\beta \to \alpha}(\{S_\beta\}|\{S_\alpha\})\, \tilde{\mathcal{H}}_{\beta \to \alpha}^{(\mathrm{1D})}\, e^{-\beta \tilde{\mathcal{H}}_{\beta \to \alpha}^{(\mathrm{1D})}}}{\sum_{\llbracket \alpha \leftrightarrow \beta \rrbracket} p_{\alpha \to \beta}(\{S_\alpha\}|\{S_\beta\})\, p_{\beta \to \alpha}(\{S_\beta\}|\{S_\alpha\})\, e^{-\beta \tilde{\mathcal{H}}_{\beta \to \alpha}^{(\mathrm{1D})}}}. \tag{9}$$

We recall here the convention adopted for the notation of the summation over the spin degrees of freedom in the expressions above:

$$\sum_{\llbracket \gamma, \delta \rrbracket_\alpha} \equiv \sum_{\substack{\{S_\gamma\}, \{S_\delta\} \\ S_{\gamma,1} = S_{\alpha,2} \\ S_{\delta,1} = S_{\alpha,3}}}, \qquad \sum_{\llbracket \beta, \gamma, \delta \rrbracket_\alpha} \equiv \sum_{\substack{\{S_\beta\}, \{S_\gamma\}, \{S_\delta\} \\ S_{\beta,1} = S_{\alpha,1} \\ S_{\gamma,1} = S_{\alpha,2} \\ S_{\delta,1} = S_{\alpha,3}}},$$

$$\sum_{\llbracket \alpha \to (\beta, \gamma, \delta) \rrbracket} \equiv \sum_{\substack{\{S_\alpha\}, \{S_\beta\}, \{S_\gamma\}, \{S_\delta\} \\ S_{\beta,1} = S_{\alpha,1} \\ S_{\gamma,1} = S_{\alpha,2} \\ S_{\delta,1} = S_{\alpha,3}}} = \sum_{\{S_\alpha\}} \sum_{\llbracket \beta, \gamma, \delta \rrbracket_\alpha},$$

$$\sum_{\llbracket \alpha \leftrightarrow \beta \rrbracket} \equiv \sum_{\substack{\{S_\alpha\}, \{S_\beta\} \\ S_{\beta,1} = S_{\alpha,1}}}. \tag{10}$$

The free energy of the system can be obtained by combining the free-energy shifts involved in the different processes, as explained in [24,52]:

$$F = \sum_{\alpha=1}^{N_\Delta} \Delta F_\alpha^{(s)} - \sum_{\langle \alpha, \beta \rangle} \Delta F_{\alpha \leftrightarrow \beta}^{(l)} = \frac{1}{2} \sum_{\langle \alpha, \beta \rangle} \left(\Delta F_{\alpha \to \beta}^{(\mathrm{iter})} + \Delta F_{\beta \to \alpha}^{(\mathrm{iter})} \right)$$

$$- \frac{1}{2} \sum_{\alpha=1}^{N_\Delta} \Delta F_\alpha^{(s)}, \tag{11}$$

where $\langle \alpha, \beta \rangle$ denotes the sum over the $3N_\Delta/2$ nearest-neighbor plaquettes on the graph (the last equality simply comes from the fact that $\Delta F_\alpha^{(s)} = \Delta F_{\alpha \to \beta}^{(\mathrm{iter})} + \Delta F_{\alpha \leftrightarrow \beta}^{(l)}$ by construction). The average entropy of the system is then given by $\langle S \rangle = \beta(\langle E \rangle - F)$. Analogously, the total average energy can be written as

$$\langle E \rangle = \sum_{\alpha=1}^{N_\Delta} \langle e_\alpha^{(s)} \rangle - \sum_{\langle \alpha, \beta \rangle} \langle e_{\alpha \leftrightarrow \beta}^{(l)} \rangle. \tag{}$$

Equations (2) can be written for arbitrary (large) RRGs and are expected to become exact in the thermodynamic limit. Since for each triangle of the RRG one can remove one of its three neighbors, Eqs. (2) represent a set of $32 \times 3 \times N_\Delta$ coupled nonlinear algebraic equations for the 32 marginal probabilities $p_{\alpha \to \beta}(\{S_\alpha\}|\{S_\beta\})$ associated to the 32 possible configurations of the spins $\{S_\alpha\}$ on the plaquette α (in absence of β), given the configuration of the spins $\{S_\beta\}$. Once the fixed points of these equations are found, one can compute the marginal probabilities on each plaquette of the graph from

Eq. (4), along with the free energy and all observables. In the following, we will discuss three specific solutions of the equations in the thermodynamic limit, corresponding to the (RS) homogeneous paramagnet, the (RS) ordered crystalline state, and the (RSB) glassy phase.

C. Paramagnetic phase

The paramagnetic phase is characterized by translational invariance and corresponds to the homogeneous and RS solution of the recursion relations:

$$p_{\alpha \to \beta}(\{S_\alpha\}|\{S_\beta\}) = p_{\mathrm{para}}(\{S_\alpha\}|\{S_\beta\}) \qquad \forall\, \alpha, \beta.$$

The probabilities $p_{\mathrm{para}}(\{S_\alpha\}|\{S_\beta\})$ are given by the fixed point of Eqs. (2) which in this limit become a simple system of 32 coupled nonlinear algebraic equations. The free energy, the energy, and the magnetization [which is identically zero by Z_2 inversion symmetry in the paramagnetic phase, which implies that $p_{\mathrm{para}}(\{S_\alpha\}|\{S_\beta\}) = p_{\mathrm{para}}(\{-S_\alpha\}|\{-S_\beta\})$], can be easily computed from Eqs. (4), (6)–(9), and (11). This phase is expected to be stable at high temperature. However, the average entropy density $\langle s \rangle = \beta(\langle e \rangle - f)$ becomes negative below a certain temperature, $T_{s=0}(D)$. This indicates that the homogeneous solution is certainly not appropriate to describe the low-temperature region of the phase diagram.

D. Stability of the paramagnetic phase

The manifestation of the failure of the RS solution also shows up via a loss of stability of the RS fixed point, as given by a simple linear analysis. To describe this instability, one needs to introduce a probability distribution $\mathcal{P}[\vec{p}]$, where $\vec{p}$ is a shorthand notation for the 32 marginal probabilities $p(\{S_\alpha\}|\{S_\beta\})$ and $\mathcal{P}[\vec{p}]$ is defined as the probability density that the probabilities $p_{\alpha \to \beta}(\{S_\alpha\}|\{S_\beta\})$ on the plaquette α (in absence of its neighboring plaquette β) are equal to $p(\{S_\alpha\}|\{S_\beta\})$.

In the homogeneous phase from Eq. (2) one has that the probability distributions of the marginal probabilities on the triangular plaquettes must satisfy the following self-consistent equation:

$$\mathcal{P}[\vec{p}] = \int d\mathcal{P}[\vec{p}_\gamma]\, d\mathcal{P}[\vec{p}_\delta]\, \delta[\vec{p} - \vec{\mathrm{p}}(\vec{p}_\gamma, \vec{p}_\delta)], \tag{12}$$

where $\vec{\mathrm{p}}(\vec{p}_\gamma, \vec{p}_\delta)$ is a shorthand notation for the right-hand side term of the recursion relations (2). Close to the homogeneous

paramagnetic solution we have, to first order,

$$p(\{S_\alpha\}|\{S_\beta\}) \approx p_{\text{para}}(\{S_\alpha\}|\{S_\beta\}) + \delta p(\{S_\alpha\}|\{S_\beta\}).$$

Starting with $\delta \vec{p}$ identically and independently distributed and injecting the expression above into Eq. (12), one has that the deviation of the marginal probabilities from the homogeneous solution evolves under iteration as

$$\langle \delta \vec{p} \rangle = 2 \left. \frac{\partial \vec{\mathrm{p}}(\vec{p}_\gamma, \vec{p}_\delta)}{\partial \vec{p}_\gamma} \right|_{\text{para}} \langle \delta \vec{p} \rangle, \qquad (13)$$

where $\langle \cdot \rangle$ refers to the average using the distribution $\mathcal{P}(\vec{p})$. $\partial \vec{\mathrm{p}} / \partial \vec{p}_\gamma$ is actually a 32×32 Jacobian matrix. If $\lambda_{\max}$ denotes the eigenvalue of largest modulus of that matrix, the stability criterion simply reads as $2|\lambda_{\max}| \leqslant 1$. When $2|\lambda_{\max}| > 1$, the paramagnetic solution is instead unstable with respect to a "modulation" instability (where $\lambda_{\max} = -\frac{1}{2}$), corresponding to a transition to a regime with successive (homogeneous) generations of the tree carrying different values of the marginal probabilities. Such modulation instability is thus a manifestation of an instability toward an ordered phase, which breaks translational invariance (more details will be given in the next section).

This instability criterion can also be obtained by studying response functions to a perturbation (which is related to correlations through the fluctuation-dissipation theorem) [24]. In this setting, the instability is detected by means of the divergence of the linear magnetic susceptibility in the paramagnetic phase, defined as

$$\chi = \frac{1}{N_\Delta} \sum_{\alpha, \beta} \langle S_\alpha S_\beta \rangle_c = \frac{1}{N_\Delta} \sum_{\alpha, \beta} \left. \frac{\partial \langle S_\alpha \rangle}{\partial h_\beta} \right|_{h_\gamma = 0},$$

where $S_\alpha \equiv \sum_{i \in \alpha} S_i$ is a shorthand notation for the magnetization of the plaquette α and h_β is an external magnetic field conjugated to the magnetization of the plaquette β. Making use of the homogeneity of the paramagnetic solution and the treelike structure of the lattice, the susceptibility can be rewritten as

$$\chi = 1 + 3 \sum_{r=1}^{\infty} 2^{r-1} \langle S_{\alpha_0} S_{\alpha_r} \rangle_c,$$

where S_{α_0} and S_{α_r} are two plaquettes taken at distance r on the tree. The series converges provided that $\lim_{r \to \infty} \log \langle S_{\alpha_0} S_{\alpha_r} \rangle_c / r < \log 2$. To evaluate $\langle S_\alpha S_\beta \rangle_c$, we invoke the fluctuation-dissipation relation

$$\langle S_{\alpha_0} S_{\alpha_r} \rangle_c = \left. \frac{\partial \langle S_{\alpha_r} \rangle}{\partial h_{\alpha_0}} \right|_{h_\gamma = 0},$$

where h_{α_0} denotes the external magnetic field conjugate to S_{α_0}. Since h_{α_0} is a function of (the components of) $P(\{S_{\alpha_0}\})$, we can use the chain rule along the branch of the tree which connects the plaquette α_0 with the plaquette α_r through the plaquettes α_l, $l = 1, \dots, r-1$:

$$\frac{\partial \langle S_{\alpha_r} \rangle}{\partial h_{\alpha_0}} = \frac{\partial \langle S_{\alpha_r} \rangle}{\partial \vec{p}_{\alpha_r \to \alpha_{r-1}}} \left(\prod_{l=2}^{r} \frac{\partial \vec{p}_{\alpha_l \to \alpha_{l-1}}}{\partial \vec{p}_{\alpha_{l-1} \to \alpha_{l-2}}} \right) \frac{\partial \vec{p}_{\alpha_1 \to \alpha_0}}{\partial \vec{P}_{\alpha_0}} \frac{\partial \vec{P}_{\alpha_0}}{\partial h_{\alpha_0}}.$$

In the paramagnetic phase, all the intermediate marginal cavity probabilities are equal and the previous equation factorizes, leading again to $2|\lambda_{\max}| \leqslant 1$.

The maximal eigenvalue $\lambda_{\max}$ decreases as the temperature is lowered and becomes equal to $-\frac{1}{2}$ at a certain temperature, signaling a modulation instability of the paramagnetic phase toward a crystalline phase (see Sec. III E) at a temperature $T_{\text{mod}}(D)$.

Below T_{mod} the linear susceptibility is given by a sum of exponentially diverging terms with alternating signs. Yet, the crystalline order of the DKIAFM is not compatible with the simplest RRG used to study the paramagnetic phase, due to the presence of loops at all scales which inhibits the periodic order to establish. As explained in the next section, in order to be able to find the crystalline phase, one needs to introduce a more complicated structure, i.e., an eight-partite RRG constructed in such a way that the specific crystalline order of the DKIAFM can establish [76].

One can also look for another kind of instability, namely, a spin-glass instability, which manifests itself as a divergence of the nonlinear susceptibility [24], which is defined as

$$\chi_{\text{sg}} = \frac{1}{N_\Delta} \sum_{\alpha, \beta} \langle S_\alpha S_\beta \rangle_c^2.$$

Equivalently, this instability appears as a widening of the variance $\langle (\delta \vec{p})^2 \rangle$ under the recursion of Eq. (12). Both approaches lead to a stability criterion $2\lambda_{\max}^2 \leqslant 1$. Note that this condition is always weaker than that for the modulation instability $2|\lambda_{\max}| \leqslant 1$, associated to the crystalline order [77]. However, it is the relevant one in the case of glassy phases, characterized by the onset of long-range amorphous order (which, contrarily to the periodic order of the crystalline phase, is compatible with the simplest RRG of triangular plaquettes).

Solving the recursion relations (2) in the paramagnetic phase, we find that the homogeneous solution becomes unstable below a temperature $T_{\text{sg}}(D)$, at which the spin-glass susceptibility diverges [with $T_{s=0}(D) < T_{\text{sg}}(D) < T_{\text{mod}}(D)$].

This requires either a phase transition *before* the spin-glass local instability is reached [[21–26] (as occurs in the mean-field models of fragile glasses, described by a random first-order transition [50,51]), or a continuous (possibly spin-glass) transition *at* T_{sg}. We will show below that the latter scenario is the correct one for the DKIAFM. In order to do this, in Sec. III F we look for a solution of the recursion relations which breaks the replica symmetry, corresponding to a glassy phase where many local minima of the free energy exist and where the local marginal probabilities fluctuate from a plaquette to another.

E. Crystal phase

The crystalline phase corresponds to a (RS) solution where the marginal probabilities do not fluctuate randomly from site to site, but are different in different sites (breakdown of translational invariance). The (sixfold-degenerate) crystalline state proposed in [48] and observed numerically in [47] is characterized by a 12-spin unit cell and breaks (twofold) time-reversal symmetry and (threefold) rotation symmetry (see Refs. [47,48] for more details). As anticipated above, this structure is not compatible with the simplest RRG used
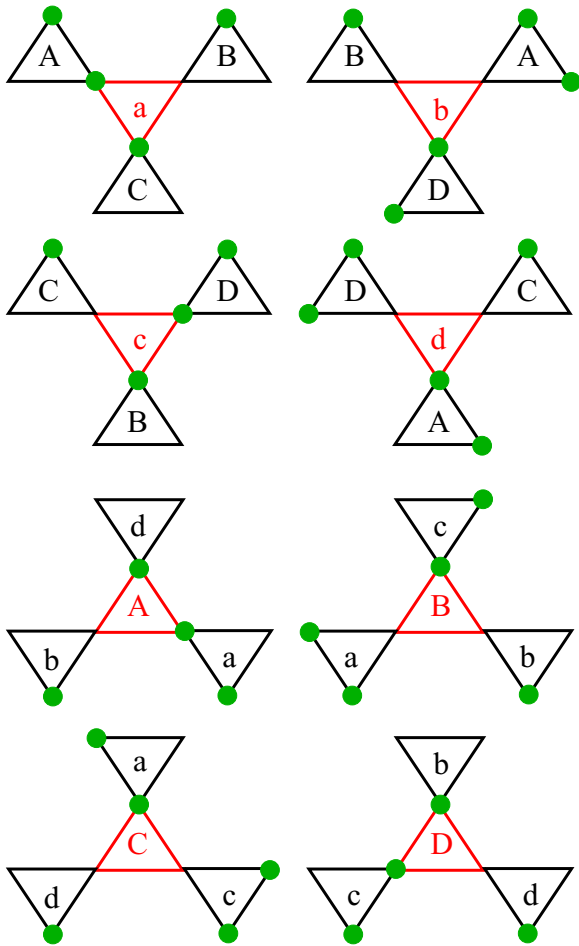
FIG. 2. Sketch of the sublattice structure introduced to describe the ordered crystalline phase proposed in [48] and detected in [47]. The four up-type plaquette sublattices are denoted by (A, B, C, D), and the four down-type plaquette sublattices are denoted by (a, b, c, d). The green circles represent the $+1$ spins in one of the sixfold-degenerate ground-state configurations. Such sublattice structure is associated to 24 different kinds of cavities, denoted by (A_n, B_n, C_n, D_n), and (a_n, b_n, c_n, d_n), with $n = 1, 2, 3$, obtained by removing one of the three neighboring plaquettes to each of the eight kinds of sublattice plaquettes. For example, the plaquette (a_1) is obtained by removing the bottom neighboring plaquette (C) from the plaquette (a), and it is connected to the plaquettes (A_3) on the right and (B_2) on the left, obtained, respectively, by removing the right neighboring plaquette (a) from the plaquette of type (A) and the left neighboring plaquette (a) from the plaquette of type (B).

to describe the paramagnetic phase, due to the presence of loops of all lengths, which inhibits the periodic order to establish. In order to be able to account for such ordered phase we need to introduce a more complicated graph, made by eight interpenetrated sublattices, labeled by the letters (A, B, C, D, a, b, c, d): each sublattice is an RRG of triangular plaquettes such that each plaquette has three randomly chosen neighboring plaquettes belonging to the other sublattices (see the caption of Fig. 2 for more details). This eight-partite RRG is built accordingly with the specific crystalline order of the DKIAFM, as illustrated in Fig. 2: for example, a site of the RRG of type (a) of down-type triangles is connected to an

up-type triangle of the RRG (A) on the up-left corner, an up-typ triangle of the RRG (B) on the up-right corner, and an up-type triangle of the RRG (C) on the bottom corner, and so on. Since for each triangle of the whole graph one can remove one of its three neighbors, this eight-partite RRG yields 24 different sets of cavity probabilities. The iteration process is done taking into account the structure of the crystalline phase, as explained in the caption of Fig. 2. The recursion equations (2) become then a set of 24×32 coupled nonlinear algebraic equations for the 24 marginal cavity probabilities on plaquettes of each sublattice in presence of a cavity. The solution of these equations appears discontinuously at a spinodal point $T_{\rm sp}(D)$, and becomes thermodynamically stable when the corresponding free energy crosses the paramagnetic one, at the melting temperature $T_m(D)$. At that temperature, we observe a first-order phase transition characterized by a spontaneous breakdown of the translational, rotational, and spin inversion invariance, accompanied by a discontinuous jump of the energy density and of the entropy density. Decreasing further the temperature, the energy in the crystalline phase approaches quickly the ground-state value $e_{\rm GS} \approx -1.6116$ (which turns out to be remarkably close to the one found with Monte Carlo simulations of systems of 300 spins, $e_{\rm GS} \approx -1.515$ [47]), and the entropy quickly approaches zero.

Note that while the translation-invariant phases can be recovered on the eight-partite RRG just by imposing that the probabilities are the same on all sublattices, the opposite is not true since the crystalline solution can only be found provided that the symmetry between the eight sublattices is broken.

Inspecting the (ground-state) spin configuration of Fig. 2, it was noticed in [47] that one of the three spins of the kagome triangles is completely polarized (i.e., the bottom spins of sublattices a, b, c, d and the top spins of sublatices A, B, C, D), with the state having zero magnetization overall. Note that the need to introduce eight sublattices of triangular plaquettes is due to the fact that the spin pattern on the two nonpolarized rows of spins of the kagome triangles (i.e., along the horizontal bonds in Fig. 2) has period four, with three spins $S = \mp 1$ followed by one spin $S = \pm 1$. Based on these observations, suitable order parameters for the transition to the ordered state are the sublattice magnetizations:

$$m_X = \sum_{i \in X} S_i,$$

with X denoting the eight different sublattices: $X = \{A, B, C, D, a, b, c, d\}$. These order parameters essentially coincide with the emergent effective charge variables introduced in Ref. [47], derived from the so-called dumbbell picture [78]. The (ground-state) spin configuration of Fig. 2 corresponds to $m_a = m_c = m_A = m_D = \pm 1$ and $m_b = m_d = m_B = m_C = \mp 1$. Equivalently, one can choose as order parameter $m_{\rm pol} = \langle S_{\rm pol} \rangle$, the average magnetization of the spins of the kagome triangles that are completely polarized, as done in [47]. Following this suggestion, we will use $|m_{\rm pol}|$ as the order parameter jumping from zero to a finite value at the transition.

We have also looked for other plausible competing ordered phases, which break the translational and rotational symmetries in different ways and have different unit cells. However, such alternative crystalline states turn out to be less favorable (i.e., they have a higher free energy)

compared to the crystalline phase of [47,48]. Yet, if one does not include the dipolar interactions between the second-nearest-neighboring plaquettes, the crystalline phase depicted in Fig. 2 disappears (i.e., no physically relevant fixed point of the recursion relations is found corresponding to the sublattice structure of Fig. 2), and another completely different (fourfold-degenerate) ordered phase emerges. This observation highlights the importance of accounting for the dipolar interaction as accurately as possible, in order to recover the correct description of the ordered phase [79].

F. Spin-glass phase

As explained above, the crystalline order of the DKIAFM cannot establish on the simple RRG which does not have the specific eight-partite structure described above. Hence, one can follow the paramagnetic solution, at least formally, in the supercooled regime $[T < T_m(D)]$, and even below the modulation instability $[T < T_{\mathrm{mod}}(D)]$ [76].

However, as mentioned above, the predicted entropy density becomes negative as the temperature is lowered below $T_{s=0}(D)$, implying that this solution does not describe well the low-temperature region. Moreover, the homogeneous solutions become unstable below a certain temperature $T_{\mathrm{sg}}(D) > T_{s=0}(D)$, at which the spin-glass susceptibility diverges. The "entropy crisis" and the spin-glass instability are manifestations of the appearance of a huge number of metastable glassy states. The RS approach fails because it does not take into account the existence of several local minima of the free energy. This requires either a phase transition before the spin-glass local instability is reached (as in the case of lattice models for fragile glasses in the mean-field limit [[21–26] described by a random first-order transition [50,51]), or a continuous spin-glass transition at T_{sg}. In order to understand which of these two possible scenarios is the correct one for the DKIAFM, we have to look for a solution of the recursion relations which breaks the replica symmetry, corresponding to a glassy phase where many local minima of the free energy exist and where the local marginal probabilities fluctuate from a plaquette to another. We thus need to perform a statistical treatment of sets of solutions of Eq. (2). The simplest setting which allows to proceed further in this direction is provided by a one-step RSB ansatz, which starts from the assumption that exponentially many (in N_Δ) solutions of the recursion relations exist. More precisely, we assume that the number $\mathcal{N}(f)$ of solutions with a given free-energy density f on graphs of size N_Δ is $\mathcal{N}(f) \sim \exp[N_\Delta \Sigma(f)]$, where $\Sigma(f) \geqslant 0$ is called the *configurational entropy* (or *complexity*) and is supposed to be an increasing and concave function of the free energy f. This is a strong hypothesis which is justified by its self-consistency. Under these assumptions, one can show that the 1RSB self-consistent equation for the probability distribution of the marginal cavity probabilities becomes [24,52]

$$\mathcal{P}_m[\vec{p}] \propto \int d\mathcal{P}_m[\vec{p}_\gamma]\, d\mathcal{P}_m[\vec{p}_\delta]\, \delta[\vec{p} - \mathrm{p}(\vec{p}_\gamma, \vec{p}_\delta)]\, e^{-\beta m \Delta F^{(\mathrm{iter})}},$$
(14)

where $\mathrm{p}(\vec{p}_\gamma, \vec{p}_\delta)$ is a shorthand notation for the right-hand side term of the recursion relations (2) and $\Delta F^{(\mathrm{iter})}$ is the free-energy shift involved in the iteration process defined in Eq. (2) via the normalization of the cavity marginal proba-

bilities. The probability distribution depends on the parameter m which is the breakpoint in Parisi's order-parameter function at the 1RSB level [24,49,52], and is defined as $m = (1/\beta)\partial\Sigma/\partial f$ (all the details of the calculation can be found in Refs. [24,26,52]). Similarly to Eq. (11), the 1RSB free-energy density functional is given by

$$\phi(m) = \Delta\phi^{(s)}(m) - \tfrac{3}{2}\Delta\phi^{(l)}(m),$$
(15)

with

$$e^{-\beta m \Delta\phi^{(s)}} = \int d\mathcal{P}_m[\vec{p}_\beta]\, d\mathcal{P}_m[\vec{p}_\gamma]\, d\mathcal{P}_m[\vec{p}_\delta]\, e^{-\beta m \Delta F^{(s)}},$$

$$e^{-\beta m \Delta\phi^{(l)}} = \int d\mathcal{P}_m[\vec{p}_\alpha]\, d\mathcal{P}_m[\vec{p}_\beta]\, e^{-\beta m \Delta F^{(l)}},$$

where the free-energy shifts have been defined in Sec. III B. The other relevant thermodynamic observables, such as, e.g., the average energy, can be obtained in a similar fashion [24,52]. The parameter m is fixed by the maximization of the free-energy functional with respect to it [24,52], which allows to recover the complexity as a Legendre transform of $\phi(m)$:

$$m\,\phi(m) = mf - \frac{1}{\beta}\Sigma(f).$$

The RS high-temperature homogeneous description of the phase is recovered by taking $P_m(\vec{p}) = \delta(\vec{p} - \vec{p}_{\mathrm{para}})$ and $m = 1$ [80].

Since Eq. (14) is a functional relation, an analytical treatment is not possible in general. Yet, the self-consistent equation can be efficiently solved numerically with arbitrary precision using a population dynamics algorithm (for all technical details, see [52]). For high values of the temperature $[T > T_{\mathrm{sg}}(D)]$ we recover the paramagnetic solution. Lowering the temperature, a nontrivial solution of the 1RSB equation appears continuously exactly at $T_{\mathrm{sg}}(D)$. Right below T_{sg} the probability distribution $\mathcal{P}_m(\vec{p})$ acquires an infinitesimal widening of the variance $\langle(\delta\vec{p})^2\rangle$. This scenario corresponds to a continuous transition to a spin-glass phase at the temperature at which the spin-glass susceptibility diverges. The order parameter of the spin-glass transition is the Edwards-Anderson order parameter $q_{\mathrm{EA}} = (1/N)\sum_i \langle S_i\rangle^2$, which vanishes linearly as $q_{\mathrm{EA}} \sim (T_{\mathrm{sg}} - T)$ for $T \to T_{\mathrm{sg}}^-$ [49].

As it is well known, the low-temperature spin-glass phase should be described by full RSB [49]. However, any new level of RSB will require considering a more sophisticated situation, namely, a distribution over the probability distribution of the previous level. For instance, the two-step RSB will be written as a distribution $\mathcal{Q}[\mathcal{P}[\vec{p}]]$ over distributions $\mathcal{P}(\vec{p})$. Describing with this formalism a finite connectivity system with full RSB is therefore too complicated, and we will limit ourselves to the 1RSB ansatz. Moreover, since solving the self-consistent functional equation (14) via population dynamics is quite computationally demanding, we did not perform the maximization of the free-energy functional (15) with respect to m. For these reasons, our approach only provides an approximate description of the equilibrium properties of the spin-glass phase and we have not pushed the 1RSB calculations far below T_{sg} (essentially we only consider few values of the temperature in the vicinity of the critical point).

IV. PHASE DIAGRAM AND THERMODYNAMIC BEHAVIOR

In this section we discuss the main results found within the mean-field treatment of the DKIAFM described in Sec. III. In order to compare with the numerical results of the Monte Carlo simulations of [47], we start by fixing the parameter D to 1, as in Refs. [47,48], and measure several observables such as the average energy density $\langle e \rangle = \langle E \rangle / N_\Delta$, the (intensive) specific heat $c = \partial \langle e \rangle / \partial T$, the magnetization of the polarized spin in one of the sixfold-degenerate ground-state configurations $|m_{pol}|$, and the average entropy density $\langle s \rangle = \langle S \rangle / N_\Delta$, as a function of the temperature T.

For the reader uninterested in the technical details of the mean-field calculations who skipped the whole Sec. III, we just recall here that one can find three different solutions of the recursive equations on the Bethe lattice:

(1) The paramagnetic state, corresponding to a translationally invariant solution where the local probabilities are the same on all the plaquettes.

(2) The spin-glass phase, corresponding to an infinite set of solutions of the mean-field recursion relations, where the probabilities fluctuate from one plaquette of the Bethe lattice to another. This infinity of possible solutions is encoded in a probability distribution obtained after averaging self-consistently over all free-energy minima with the corresponding Gibbs weight. After averaging over all free-energy minima, the probability distributions over all possible solutions are again translationally invariant.

(3) The crystal phase, where the local probabilities do not fluctuate randomly from one plaquette to another, but are different on different plaquettes (breakdown of translational invariance).

The paramagnetic and spin-glass phases are found on simple RRGs of triangular plaquettes, while the crystalline order can only establish on a more complicated eight-partite RRG constituted by eight sublattices.

The results are shown in Fig. 3. At high temperature the system is found in the paramagnetic phase. Upon lowering the temperature, a first-order transition to the crystalline phase proposed in Refs. [47,48] (see Fig. 2) occurs at T_m. The order parameter $|m_{pol}|$ presents a finite jump at T_m, where the average energy and entropy densities also display an abrupt drop. The transition to the ordered state turns out to be weakly first order, in the sense that the spinodal point of the crystalline solution $T_{sp} \approx 0.16$ K is very close to the transition temperature $T_m \approx 0.1566$ K where the free energies of the paramagnetic phase and the crystal phase cross. The modulation instability where the paramagnetic phase would become unstable toward the crystalline phase is instead found at significantly lower temperature $T_{mod} \approx 0.147$ K. Since the specific heat of the crystal solution diverges at the spinodal point, the vicinity of T_m and T_{sp} results in a very large jump (of about a factor 3) of the intensive specific heat at the transition. This feature might explain the deviations observed in the numerical simulations from the expected scaling of the peak of the (extensive) specific heat as $C_{max} \propto N_\Delta$ [47]. (On the other hand, on the high-temperature paramagnetic side of the transition the specific heat is featureless in the vicinity of T_m.)

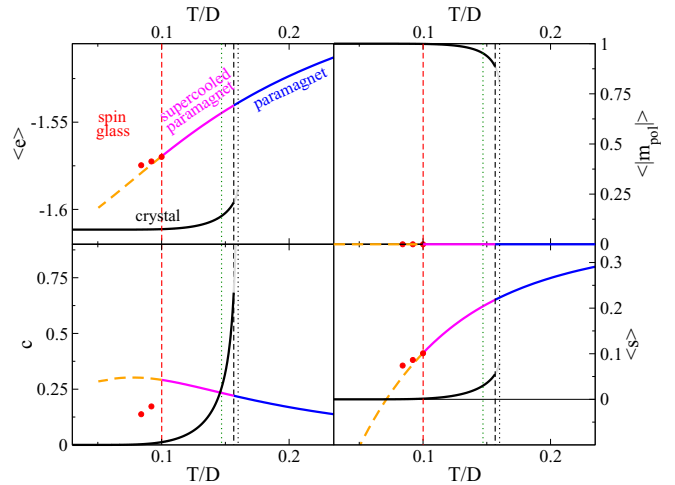Although approximate, our approach accounts remarkably well for the numerical results of Ref. [47]. As expected,

FIG. 3. Average energy density $\langle e \rangle$ (top left), magnetization of the polarized spins $|m_{pol}|$ (top right), specific heat (per plaquette) $c = \partial \langle e \rangle / \partial T$ (bottom left), and average entropy density $\langle s \rangle$ (bottom right) as a function of the temperature T for $J = 0.5$ and $D = 1$. Data in the paramagnetic phase are shown in blue, in the crystal phase in black, in the supercooled paramagnetic phase in magenta. The red circles are obtained by solving the 1RSB equations in the spin-glass phase (with $m = 1$). The vertical dashed black and red lines correspond to the first-order transition to the crystal state at T_m and the continuous transition to the spin-glass phase at T_{sg}, respectively. The gray curves correspond to the crystal solution in the metastable region and end at the spinodal point (T_{sp}, vertical black dotted line). The green dotted vertical line gives the position of the modulation instability of the homogeneous solution T_{mod}. The orange dashed curves correspond to the (unstable) RS solution of the equation below the spin-glass transition point, and show the entropy crisis in the manner of Kauzmann of the RS solution (at $T_{s=0}$).

the transition temperature is overestimated by the mean-field approximation (by about a factor 3). Yet, the temperature dependencies of the specific heat, the energy, and the magnetization are, also at a quantitative level, very similar to the ones found in Ref. [47] (recall that the energy, entropy, and specific heat *per spin* are obtained by multiplying the energy, entropy, and specific heat *per plaquette* by a factor $\frac{2}{3}$).

Since the crystalline order of the DKIAFM cannot establish on the simple RRG which does not have the specific eight-partite structure described in Sec. III E, one can follow the paramagnetic solution in the supercooled regime ($T < T_m$) even below the modulation instability ($T < T_{mod}$) [76]. If one keeps lowering the temperature, the spin-glass susceptibility grows and diverges at $T_{sg} \approx 0.1$ K, where a continuous transition to a spin-glass phase takes place. Although the spin-glass phase is presumably described by full RSB (at least at the mean-field level), our approach only allows one to perform an approximate 1RSB ansatz for the low-temperature glassy phase. Moreover, solving the self-consistent functional equation (14) via population dynamics is computationally heavy. For these reasons, we did not push the calculations of the thermodynamic observables too deep into the spin-glass phase, and only solved the equations for few points close to the critical temperature.
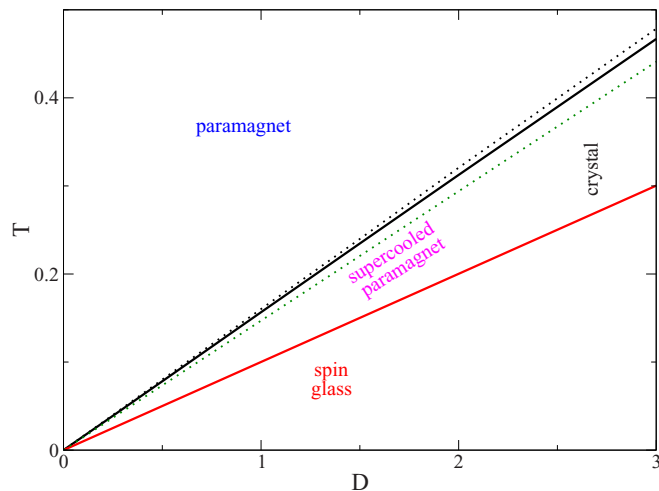
FIG. 4. Mean-field phase diagram of the model in the D-T plane for $J = 0.5$, showing the position of the different phases and the transition lines. The black continuous line corresponds to the first-order melting transition $T_m(D)$, where the free energies of the paramagnetic and the crystalline solutions cross. The black dotted line gives the spinodal point at which the crystalline solution appears discontinuously. The green dotted line corresponds to the modulation instability of the paramagnetic solution $T_{\mathrm{mod}}(D)$. The red continuous line is the continuous spin-glass transition $T_{\mathrm{sg}}(D)$, where the spin-glass susceptibility diverges.

Since the kagome lattice *is* compatible with the crystalline ground state of the DKIAFM, one might expect that the paramagnetic phase should in fact disappear below T_{mod}. However, one should keep in mind that there are some frustrated Ising models (see, e.g., Ref [35]) for which the transition to the ordered phase becomes more discontinuous in finite dimension compared to their mean-field counterpart. It is therefore possible that in 2D T_{mod} is shifted to lower temperature (relatively to T_m). In this case, the supercooled paramagnetic phase which exists between $T_{\mathrm{mod}} < T < T_m$ might be strongly influenced by the remnant of a spin-glass transition found at the mean-field level since the spin-glass susceptibility might be already very large a T_{mod}.

In Fig. 4 we plot the phase diagram of the DKIAFM, showing the position of the different phases when varying the temperature T and the dipolar interaction D (J is fixed to $J = 0.5$ K). The effect of varying the dipolar interaction is particularly simple. In fact, we find that the phase boundaries, as well as all the characteristic temperature scales, vary linearly with D:

$$T_m \approx 0.1566D,$$
$$T_{\mathrm{sg}} \approx 0.1\,D,$$
$$T_{\mathrm{sp}} \approx 0.16\,D,$$
$$T_{\mathrm{mod}} \approx 0.147\,D,$$
$$T_{s=0} \approx 0.0713\,D.$$

As expected, in the limit $D = 0$ the paramagnetic phase is stable at all temperatures and corresponds to the only solution of the recursion relations. This is due to the fact that for $D = 0$ the system is much less frustrated and has a highly

(i.e., extensively) degenerate ground state (i.e., $\langle s \rangle$ approaches a finite value in the $T \to 0$ limit) since each plaquette has a sixfold-degenerate ground state which corresponds to the ice rule (two $+1$ and one -1 spins or two -1 and one $+1$ spins). In particular, for $D = 0$ the model reduces to the nearest-neighbor kagome spin-ice model of Wills, Ballou, and Lacroix [59], for which a Pauling estimate yields the entropy $s_{\mathrm{GS}} = (3/2) \log[2(3/4)^{2/3}] \approx 0.752\,25$, while our mean-field approximation yields $s_{\mathrm{GS}} \approx 0.752\,04$. When the dipolar interactions are turned on ($D > 0$), such degeneracy is lifted, and a specific crystalline ground-state structure emerges. The minimization of the local interactions produces a much stronger geometric frustration for $T \lesssim D$ and gives rise to the emergence of a spin-glass phase at low temperatures, characterized by an extremely rough free-energy landscape (at least at the mean-field level). The fact that all the relevant temperature scales of the problem show an apparent linear dependence on D is precisely due to the fact that the relevant energy scale is the energy difference between the ground state and the first excited states, which goes linearly to zero with D.

V. CONCLUSIONS

In this paper we have developed an analytical mean-field treatment for the equilibrium properties of the DKIAFM introduced in [48] and studied numerically in [47]. Our mean-field approach is based on a cluster variational Bethe-Peierls formalism [4,71–74] and on the cavity method [52], and consists in studying the model on a sparse random tree-like graph of triangular kagome plaquettes, and cutting off the dipolar interaction beyond the second-nearest-neighbor plaquettes (i.e., the fifth-nearest-neighbor spins). Our results essentially confirm and support the observations reported in Ref. [47], which were obtained using Monte Carlo simulations of relatively small system (ranging from 48 to 300 spins), and might be affected by both strong finite-size effects and by the difficulty of reaching thermal equilibrium in a reliable fashion due to strong metastability effects.

The summary of our results is the following. Upon decreasing the temperature, we first find a transition to a sixfold-degenerate crystal state which breaks time-reversal, translation, and rotation symmetry as the one proposed in [47,48]. Such transition is indeed discontinuous, as suggested in [47], although its first-order character turns out to be weak, which might explain the strong finite-size effects observed in the finite-size scaling of the numerical data of the specific heat. When the system is supercooled below the first-order transition, we find that the paramagnetic state becomes unstable below a temperature at which the spin-glass susceptibility diverges and a continuous spin-glass transition takes place at the mean-field level. The remnant of such spin-glass transition could be detected in numerical simulations and experimental realizations of the DKAIFM by measuring the nonlinear susceptibility [81].

On the one hand, the results presented here support and clarify the numerical findings of Ref. [47]. On the other hand, they provide a first step to bridge the gap between the slow dynamics observed in geometrically frustrated magnetic systems and the mean-field theory of glassy systems formulated in terms of rough free-energy landscape. We believe

that this analysis is of particular interest, especially in the light of the experimental relevance of the model, which could be potentially realized in several realistic setups, including colloidal crystals [61,62,82–85], artificial nanomagnetic arrays [63,64,86,87], polar molecules [65], atomic gases with large magnetic dipole moments [66], and layered bulk kagome materials [67–69].

Some comments are now in order.

The lower critical dimension of the spin-glass transition is expected to be $d_L \approx 2.5$ [55] (at least in the case of short-range interactions). Hence, we do not expect a genuine spin-glass phase for the DKIAFM. Yet, in 2D the spin-glass amorphous order can establish over very large (although not infinite) length scales and the spin-glass susceptibility can become very large (although not infinite) at low temperature due to the vestiges of the transition. Indeed, there are plenty of experimental studies using thin films that at sufficiently low temperatures behave as the 3D counterparts. See, e.g., [57] for a very recent reference and [56] for a more classical ones. The situation is similar concerning numerical simulations [58]. Furthermore, since $T_{\rm sg} < T_{\rm mod}$, our mean-field analysis seems to suggest that the spin-glass phase could not be realized because the paramagnetic one becomes unstable at higher temperatures [77]. Yet, as there are models (like in [35]) which are more discontinuous in finite dimensions with respect to their mean-field counterpart, it is possible that $T_{\rm mod}$ can decrease (relatively to T_m) in 2D compared to the mean-field solution. Hence, the properties of the supercooled paramagnet below T_m could be influenced by the fact that the spin-glass susceptibility is already very large at $T_{\rm mod}$.

Concerning the dynamics, very early Monte Carlo simulations of the 3D Edwards-Anderson model suggested that the spin autocorrelation function, close but above the expected critical temperature, decays as a stretched exponential [53]. Therefore, although the the spin-glass transition is a second-order phase transition with critical slowing down and algebraic decay of correlation functions, for the system sizes and timescales accessed in Ref. [53], the time-delayed correlations were satisfactorily fitted by such an anomalous form, with a stretching exponent decaying with decreasing temperature. Just a bit later, in [54] the conventional critical slowing down was recovered. A stretched exponential relaxation of the self-correlation in the DKIAFM was reported in [47]. However, although the origin of stretched exponential relaxations in the 3D Edwards-Anderson model and in fragile glass formers is of different nature, for limited system sizes it is hard to distinguish sharply between this behavior and a slow algebraiclike decay.

The case $J = 0$ and $D > 0$ [70] has been left over by the present investigation and might be an interesting subject for future studies. Possibly, the most interesting questions would be the investigation of how the properties of the model are affected by quantum fluctuations.

APPENDIX: ANTIFERROMAGNETIC ISING MODEL ON THE RRG

The solution of the DKIAFM on the Bethe lattice shares many similarities with other geometrically frustrated models whose mean-field version on sparse random networks exhibits a spin-glass phase. In this Appendix we discuss the simplest example, which is provided by the Ising model with antiferromagnetic interactions, which we believe can help the reader to get a better intuition of the results described in the main text and of their physical implications. The Hamiltonian of the model is

$$\mathcal{H} = J \sum_{\langle i,j \rangle} S_i S_j,$$

with $J > 0$. This model can be easily solved on a RRG of connectivity $k + 1$. The recursion equations, i.e., the equivalent of Eqs. (2) for the probabilities $p_{i \to j}$ and $q_{i \to j} = 1 - p_{i \to j}$, of the spin i being up or down in absence of one of its $k + 1$ neighbors j, are

$$p_{i \to j} = \frac{1}{\mathcal{Z}_{i \to j}^{\rm (iter)}} \prod_{m \in \partial i/j} (e^{-\beta J} p_{m \to i} + e^{\beta J} q_{m \to i}),$$

$$q_{i \to j} = \frac{1}{\mathcal{Z}_{i \to j}^{\rm (iter)}} \prod_{m \in \partial i/j} (e^{-\beta J} q_{m \to i} + e^{\beta J} p_{m \to i}), \quad \text{(A1)}$$

where the notation $m \in \partial i/j$ indicates the set of all neighbors of i but j, and $\mathcal{Z}_{i \to j}^{\rm (iter)}$ is the normalization factor which ensures that $p_{i \to j} + q_{i \to j} = 1$.

The paramagnetic phase is obtained by imposing translation invariance, i.e., $p_{i \to j} = p \; \forall \; (i, j)$, which yields

$$p = \frac{[e^{\beta J} - 2p \sinh(\beta J)]^k}{[e^{\beta J} - 2p \sinh(\beta J)]^k + [e^{-\beta J} + 2p \sinh(\beta J)]^k}. \quad \text{(A2)}$$

It is straightforward to show that for any value of βJ the equation above admit the unique solution $p = \frac{1}{2}$ (i.e., $m = 0$).

In order to study the stability of the paramagnetic phase, similarly to Eq. (13), one has to compute the derivative $dp_{i \to j}/dp_{m \to i}|_{p=1/2} = -\tanh(\beta J) \equiv \lambda$. The correlation function between two spins at distance r on the RRG is thus

$$\langle S_i S_{i+r} \rangle = [-\tanh(\beta J)]^r,$$

which yields the linear and spin-glass susceptibilities as

$$\chi = 1 + \frac{k+1}{k} \sum_r [-k \tanh(\beta J)]^r,$$

$$\chi_{\rm sg} = 1 + \frac{k+1}{k} \sum_r [k \tanh^2(\beta J)]^r.$$

At temperature $T_{\rm mod} = J/\text{atanh}(1/k)$ the paramagnetic phase exhibits a modulation instability (for any $k > 1$) toward an antiferromagnetic phase where χ diverges. The spin-glass susceptibility also diverges at a lower temperature $T_{\rm sg} = J/\text{atanh}(1/\sqrt{k})$. The modulation instability is the manifestation of a second-order transition to an antiferromagnetic phase, characterized by a staggered order, where each $\uparrow$ spin is surrounded by $k + 1$ $\downarrow$ spins and so on. However, this phase can only be realized on bipartite lattices. The simple RRG is not bipartite due to the presence of loops of all

lengths [88]. Hence, the antiferromagnetic order cannot be realized on these lattices. Yet, one can find an antiferromagnetic solution by introducing a more complicated graph, made of two interpenetrated RRGs labeled by the letters (A) and (B), and constructed in such a way that each site of (A) is connected to $k + 1$ randomly chosen sites of (B) and each site of (B) is connected to $k + 1$ randomly chosen sites of (A). Imposing translation invariance separately on the (A) and (B) sublattices, Eqs. (A1) become

$$p_a = \frac{[e^{\beta J} - 2p_b \sinh(\beta J)]^k}{[e^{\beta J} - 2p_b \sinh(\beta J)]^k + [e^{-\beta J} + 2p_b \sinh(\beta J)]^k},$$

$$p_b = \frac{[e^{\beta J} - 2p_a \sinh(\beta J)]^k}{[e^{\beta J} - 2p_a \sinh(\beta J)]^k + [e^{-\beta J} + 2p_a \sinh(\beta J)]^k}.$$

Of course, above T_{mod} the paramagnetic solution can be simply recovered imposing $p_a = p_b$. However, below T_{mod} another solution appears continuously where translational invariance is spontaneously broken [89].

As said above, this solution does not exist on the simple nonbipartite RRGs. One can thus follow, at least formally, the paramagnetic solution down to T_{sg}. Here, a spin-glass transition (described by full RSB) occurs. This is signaled by the

appearance of an infinity of solutions of Eqs. (A1) where the local probabilities fluctuate from site to site. Proper averaging over all solutions (i.e., all minima of the free energy) at the 1RSB level yields

$$\mathcal{P}_m(p) = \int \prod_{m=1}^{k} d\mathcal{P}_m(p_i)\delta[p - f(\{p_m\})]\big(\mathcal{Z}_m^{(\text{iter})}\big)^m,$$

where the function $f(\{p_m\})$ represents the right-hand side of Eq. (A1).

One can of course ask what is the relevance of this spin-glass transition since it occurs in a temperature range where the paramagnetic phase seems to be unstable anyway. The answer depends on the physical situation that one wants to describe. For example, 2D square lattices are bipartite and no paramagnetic state can exist below T_{mod}. On the contrary, triangular lattices are not bipartite and the antiferromagnetic order cannot establish [yet one still finds a modulation instability on RRGs of connectivity $k + 1 = 3$ at $T_{\text{mod}} = J/\text{atanh}(\frac{1}{2})$]. The existence of a spin-glass solution at low temperature in this case reflects somehow the fact that the Ising model with antiferromagnetic interactions becomes highly frustrated at low T on a triangular lattice (although no true spin-glass transition can occur in 2D anyway).

[1] G. Toulouse, Commun. Phys. **2**, 115 (1977).

[2] L. Balents, Nature (London) **464**, 199 (2010).

[3] R. Moessner and A. P. Ramírez, Phys. Today **59**(2), 24 (2006).

[4] L. D. C. Jaubert, J. T. Chalker, P. C. W. Holdsworth, and R. Moessner, Phys. Rev. Lett. **100**, 067207 (2008).

[5] E. H. Lieb and F. Y. Wu, in *Phase Transitions and Critical Phenomena*, edited by C. Domb and J. L. Lebowitz (Academic, New York, 1972), Vol. 1, Chap. 8, p. 331.

[6] R. Youngblood, J. D. Axe, and B. M. McCoy, Phys. Rev. B **21**, 5212 (1980).

[7] C. Henley, Annu. Rev. Condens. Matter Phys. **1**, 179 (2010).

[8] P. G. Wolynes and V. Lubchenko, *Structural Glasses and Super-cooled Liquids: Theory, Experiment, and Applications* (Wiley, Hoboken, NJ, 2012).

[9] L. Berthier and G. Biroli, Rev. Mod. Phys. **83**, 587 (2011).

[10] A. Cavagna, Phys. Rep. **476**, 51 (2009).

[11] W. Götze, in *Liquids, Freezing and the Glass Transition*, edited by J. P. Hansen, D. Levesque, J. Zinn-Justin, and Les Houches, Session LI, 1989 (North-Holland, Amsterdam, 1991).

[12] P. G. Debenedetti, *Metastable Liquids* (Princeton University Press, Princeton, NJ, 1996).

[13] G. Tarjus, in *Dynamical Heterogeneities in Glasses, Colloids, and Granular Media*, edited by L. Berthier, G. Biroli, J.-P. Bouchaud, L. Cipelletti, and W. van Saarloos (Oxford University Press, New York, 2011), Chap. 2.

[14] E. Marinari, G. Parisi, and F. Ritort, J. Phys. A: Math. Gen. **27**, 7615 (1994); **27**, 7647 (1994).

[15] J.-P. Bouchaud and M. Mézard, J. Phys. I **4**, 1109 (1994).

[16] L. F. Cugliandolo, J. Kurchan, G. Parisi, and F. Ritort, Phys. Rev. Lett. **74**, 1012 (1995).

[17] J.-P. Bouchaud, L. F. Cugliandolo, J. Kurchan, and M. Mézard, Physica A (Amsterdam) **226**, 243 (1996).

[18] M. Grousson, G. Tarjus, and P. Viot, Phys. Rev. E **65**, 065103(R) (2002); J. Phys.: Condens. Matter **14**, 1617 (2002).

[19] G. Tarjus, S. A. Kivelson, Z. Nussinov, and P. Viot, J. Phys.: Condens. Matter **17**, R1143(R) (2005).

[20] J. Schmalian and P. G. Wolynes, Phys. Rev. Lett. **85**, 836 (2000); H. Westfahl, J. Schmalian, and P. G. Wolynes, Phys. Rev. B **64**, 174203 (2001).

[21] G. Biroli and M. Mézard, Phys. Rev. Lett. **88**, 025501 (2001).

[22] M. P. Ciamarra, M. Tarzia, A. de Candia, and A. Coniglio, Phys. Rev. E **67**, 057105 (2003); **68**, 066111 (2003).

[23] M. Weigt and A. K. Hartmann, Europhys. Lett. **62**, 533 (2003).

[24] O. Rivoire, G. Biroli, O. C. Martin, and M. Mézard, Eur. Phys. J. B **37**, 55 (2004).

[25] M. Tarzia, J. Stat. Mech. (2007) P01010.

[26] F. Krząkała and L. Zdeborová, Europhys. Lett. **81**, 57005 (2008); L. Zdeborová and F. Krzakala, Phys. Rev. E **76**, 031131 (2007).

[27] J. Kurchan, G. Parisi, and F. Zamponi, J. Stat. Mech. (2012) P10012; J. Kurchan, G. Parisi, P. Urbani, and F. Zamponi, J. Phys. Chem. B **117**, 12979 (2013); P. Charbonneau, J. Kurchan, G. Parisi, P. Urbani, and F. Zamponi, J. Stat. Mech. (2014) P10009; Annu. Rev. Condens. Matter Phys. **8**, 265 (2017); T. Maimbourg, J. Kurchan, and F. Zamponi, Phys. Rev. Lett. **116**, 015902 (2016).

[28] F. Ritort and P. Sollich, Adv. Phys. **52**, 219 (2003).

[29] D. Chandler and J. P. Garrahan, Annu. Rev. Phys. Chem. **61**, 191 (2010).

[30] J. P. Garrahan and M. E. J. Newman, Phys. Rev. E **62**, 7670 (2000).

[31] J. P. Garrahan, Phys. Rev. E **89**, R030301(R) (2014); R. M. Turner, R. L. Jack, and J. P. Garrahan, *ibid.* **92**, 022115 (2015); R. L. Jack and J. P. Garrahan, Phys. Rev. Lett. **116**, 055702 (2016).

[32] J. D. Shore, M. Holzer, and J. P. Sethna, Phys. Rev. B **46**, 11376 (1992).

[33] S. A. Cannas, M. F. Michelon, D. A. Stariolo, and F. A. Tamarit, Phys. Rev. E **78**, 051602 (2008).

[34] O. Osenda, F. A. Tamarit, and S. A. Cannas, Phys. Rev. E **80**, 021114 (2009).

[35] D. Kivelson, S. A. Kivelson, X. L. Zhao, Z. Nussinov, and G. Tarjus, Physica A (Amsterdam) **219**, 27 (1995).

[36] I. Esterlis, S. A. Kivelson, and G. Tarjus, Phys. Rev. B **96**, 144305 (2017).

[37] O. Cépas and B. Canals, Phys. Rev. B **86**, 024434 (2012).

[38] O. Cépas, Phys. Rev. B **90**, 064404 (2014).

[39] S. Mahmoudian, L. Rademaker, A. Ralko, S. Fratini, and V. Dobrosavljevic, Phys. Rev. Lett. **115**, 025701 (2015).

[40] Z. Budrikis, K. L. Livesey, J. P. Morgan, J. Akerman, A. Stein, S. Langridge, C. H. Marrows, and R. L. Stamps, New J. Phys. **14**, 035014 (2012).

[41] D. Levis and L. F. Cugliandolo, Europhys. Lett. **97**, 30002 (2012); Phys. Rev. B **87**, 214302 (2013).

[42] M. J. Harris, S. T. Bramwell, D. F. McMorrow, T. Zeiske, and K. W. Godfrey, Phys. Rev. Lett. **79**, 2554 (1997).

[43] M. Alba, J. Hammann, C. Jacoboni, and C. Pappa, Phys. Lett. A **89**, 423 (1982); J. Greedan, M. Sato, X. Yan, and F. Razavi, Solid State Commun. **59**, 895 (1986); J. N. Reimers, J. E. Greedan, R. K. Kremer, E. Gmelin, and M. A. Subramanian, Phys. Rev. B **43**, 3387 (1991); M. J. P. Gingras, C. V. Stager, N. P. Raju, B. D. Gaulin, and J. E. Greedan, Phys. Rev. Lett. **78**, 947 (1997); J. S. Gardner, B. D. Gaulin, S. H. Lee, C. Broholm, N. P. Raju, and J. E. Greedan, *ibid.* **83**, 211 (1999); H. Zhou, C. Wiebe, A. Harter, N. Dalal, and J. S. Gardner, J. Phys.: Condens. Matter **20**, 325201 (2008); T. Taniguchi, T. Munenaka, and H. Sato, J. Phys.: Confer. Ser. **145**, 012017 (2009); F. Ladieu, F. Bert, V. Dupuis, E. Vincent, and J. Hammann, J. Phys.: Condens. Matter **16**, S735 (2004).

[44] K. Mitsumoto, C. Hotta, and H. Yoshino, Phys. Rev. Lett. **124**, 087201 (2020).

[45] S. Edwards and P. W. Anderson, J. Phys. F: Met. Phys. **5**, 965 (1975).

[46] M. Tarzia and G. Biroli, Europhys. Lett. **82**, 67008 (2008).

[47] J. Hamp, R. Moessner, and C. Castelnovo, Phys. Rev. B **98**, 144439 (2018).

[48] I. A. Chioar, N. Rougemaille, and B. Canals, Phys. Rev. B **93**, 214410 (2016).

[49] M. Mézard, G. Parisi, and M. A. Virasoro, *Spin Glass Theory and Beyond* (World Scientific, Singapore, 1987).

[50] T. R. Kirkpatrick, D. Thirumalai, and P. G. Wolynes, Phys. Rev. A **40**, 1045 (1989).

[51] V. Lubchenko and P. G. Wolynes, Annu. Rev. Phys. Chem. **58**, 235 (2007).

[52] M. Mézard and G. Parisi, Eur. Phys. J. B **20**, 217 (2001).

[53] A. T. Ogielski, Phys. Rev. B **32**, 7384 (1985).

[54] A. T. Ogielski and I. Morgenstern, Phys. Rev. Lett. **54**, 928 (1985).

[55] S. Franz, G. Parisi, and M. A. Virasoro, J. Phys. I **4**, 1657 (1994); V. Astuti, S. Franz, and G. Parisi, J. Phys. A: Math. Theor. **52**, 294001 (2019).

[56] J. Mattsson, P. Granberg, P. Nordblad, L. Lundgren, R. Loloee, R. Stubi, J. Bass, and J. A. Cowen, J. Magn. Magn. Mater. **104**, 1623 (1992).

[57] S. Guchhait and R. L. Orbach, Phys. Rev. Lett. **118**, 157203 (2017).

[58] L. A. Fernández, E. Marinari, V. Martín-Mayor, G. Parisi, and J. J. Ruiz-Lorenzo, J. Phys. A: Math. Theor. **52**, 224002 (2019).

[59] A. S. Wills, R. Ballou, and C. Lacroix, Phys. Rev. B **66**, 144407 (2002).

[60] Note that the fact that the mean-field value of the ground-state energy is found to be lower than the 2D value is due to the fact that the dipolar interactions are cut off beyond the second-nearest-neighbor plaquettes in the mean-field calculations.

[61] Y. Han, Y. Shokef, A. M. Alsayed, P. Yunker, T. C. Luben-sky, and A. G. Yodh, Nature (London) **456**, 898 (2008).

[62] D. Zhou, F. Wang, B. Li, X. Lou, and Y. Han, Phys. Rev. X **7**, 021030 (2017).

[63] I. A. Chioar, N. Rougemaille, A. Grimm, O. Fruchart, E. Wagner, M. Hehn, D. Lacour, F. Montaigne, and B. Canals, Phys. Rev. B **90**, 064411 (2014).

[64] C. Nisoli, R. Moessner, and P. Schiffer, Rev. Mod. Phys. **85**, 1473 (2013).

[65] K.-K. Ni, S. Ospelkaus, M. H. G. de Miranda, A. Pe'er, B. Neyenhuis, J. J. Zirbel, S. Kotochigova, P. S. Julienne, D. S. Jin, and J. Ye, Science **322**, 231 (2008).

[66] A. Griesmaier, J. Werner, S. Hensler, J. Stuhler, and T. Pfau, Phys. Rev. Lett. **94**, 160401 (2005).

[67] A. Scheie, M. Sanders, J. Krizan, Y. Qiu, R. J. Cava, and C. Broholm, Phys. Rev. B **93**, 180407(R) (2016).

[68] J. A. M. Paddison, H. S. Ong, J. O. Hamp, P. Mukherjee, X. Bai, M. G. Tucker, N. P. Butch, C. Castelnovo, M. Mourigal, and S. E. Dutton, Nat. Commun. **7**, 13842 (2016).

[69] Z. L. Dun, J. Trinh, M. Lee, E. S. Choi, K. Li, Y. F. Hu, Y. X. Wang, N. Blanc, A. P. Ramirez, and H. D. Zhou, Phys. Rev. B **95**, 104439 (2017).

[70] T. Takagi and M. Mekata, J. Phys. Soc. Jpn. **62**, 3943 (1993).

[71] D. Levis, L. F. Cugliandolo, L. Foini, and M. Tarzia, Phys. Rev. Lett. **110**, 207206 (2013).

[72] L. Foini, D. Levis, M. Tarzia, and L. F. Cugliandolo, J. Stat. Mech. (2013) P02026.

[73] L. F. Cugliandolo, G. Gonnella, and A. Pelizzola, J. Stat. Mech. (2015) P06008.

[74] E. N. M Cirillo, G. Gonnella, D. A. Johnston, and A. Pelizzola, Phys. Lett. A **226**, 59 (1997); A. Pelizzola, J. Phys. A: Math. Gen. **38**, R309(R) (2005).

[75] N. C. Wormald, in *Surveys in Combinatorics*, edited by J. D. Lamb and D. A. Preece, London Mathematical Society Lecture Note Series Vol. 276 (Cambridge University Press, Cambridge, 1999), p. 239.

[76] Yet, below T_{mod} this instability manifests itself in the fact that in order to find the paramagnetic fixed point of Eqs. (2) iteratively, one needs to introduce a dumping to ensure numerical convergence.

[77] It can be generically shown for models with a spin-glass transition on treelike graphs that, since $\chi \simeq \sum_r (k\lambda_{max})^r$ and $\chi_{sg} \simeq \sum_r (k\lambda_{max}^2)^r$ ($k + 1$ being the connectivity of the graph), the spin-glass susceptibility is bounded by the square of the linear susceptibility and no divergence of the former can occur without a divergence of the latter.

[78] C. Castelnovo, R. Moessner, and S. L. Sondhi, Nature (London) **451**, 42 (2008).

[79] P. Andriushchenko, J. Magn. Magn. Mater. **476**, 284 (2019).

[80] In particular, it can be shown that $m = 1$ always gives back the paramagnetic RS solution.

[81] K. Binder and A. Young, Rev. Mod. Phys. **58**, 801 (1986).

[82] A. Le Cunuder, I. Frerot, A. Ortíz-Ambriz, and P. Tierno, Phys. Rev. B **99**, 180504(R) (2019).

[83] J. Loehr, A. Ortíz-Ambriz, and P. Tierno, Phys. Rev. Lett. **117**, 168001(R) (2016).

[84] A. Ortíz-Ambriz and P. Tierno, Nat. Commun. **7**, 10575 (2016).

[85] A. Libal, C. J. O. Reichhardt-Olson, and C. Reichhardt, New J. Phys. **17**, 103010 (2015).

[86] A. Farhan, P. M. Derlet, A. Kleibert, A. Balan, R. V. Chopdekar, M. Wyss, J. Perron, A. Scholl, F. Nolting, and L. J. Heyderman, Phys. Rev. Lett. **111**, 057204 (2013); A. Farhan, A. Kleibert, P. M. Derlet, L. Anghinolfi, A. Balan, R. V. Chopdekar, M.

Wyss, S. Gliga, and F. Nolting, and L. J. Heyderman, Phys. Rev. B **89**, 214405 (2014).

[87] O. Sendetskyi, V. Scagnoli, N. Leo, L. Anghinolfi, A. Alberca, J. Luning, U. Staub, P. M. Derlet, and L. J. Heyderman, Phys. Rev. B **99**, 214430 (2019).

[88] Note that contrary to the RRG, the loopless Cayley tree is instead bipartite.

[89] Note that the $\mathbb{Z}_2$ symmetry imposes that $p_a = 1 - p_b$. One thus find that p_a satisfies Eq. (A2) with $J \to -J$, which gives back the solution of the ferromagnetic Ising model on each sublattice with $m_a = -m_b$.